Engineering Structures 174 (2018) 462–477

Contents lists available at ScienceDirect

Engineering Structures

journal homepage: www.elsevier.com/locate/engstruct

Wind-load fragility analysis of monopole towers by Layered Stochastic-Approximation-Monte-Carlo method

Gian Felice Giaccu[a], Luca Caracoglia[b,*]

[a] Department of Architecture, Design and Urban Planning, University of Sassari, Palazzo del Pou Salit, Piazza Duomo 6, 07041 Alghero, Italy
[b] Department of Civil and Environmental Engineering, Northeastern University, 360 Huntington Avenue, Boston, MA 02115, USA

ARTICLE INFO

Keywords:
Slender structures
Wind loading uncertainties
Along-wind dynamic response
Stochastic approximation
Monte Carlo method
First-order reliability method

ABSTRACT

This paper describes a novel numerical algorithm for the simulation of the along-wind dynamic response of a prototype of slender towers under turbulent winds, using a Layered Stochastic Approximation Monte Carlo algorithm (LSAMC). The proposed algorithm is applied to derive the statistics of the dynamic response in the presence of uncertainties in the structural properties and in the wind loading. Standard "brute force" Monte-Carlo methods are also used for validating the LSAMC results. The proposed methodology efficiently estimates structural fragility curves under extreme wind loads. The methodology enables a significant speedup in the computing time compared to standard Monte Carlo sampling. Furthermore, it is demonstrated that accuracy in the estimation of structural fragility curves is superior to ordinary reliability methods (e.g. "First-order reliability methods" or FORM).

1. Introduction

Comprehensive research activities in the recent past have been undertaken in the area of risk-based assessment of structural integrity with a specific focus on earthquake engineering (performance-based engineering) [1]. In performance-based engineering, the basic idea is to ensure that a structure, for example subjected to various hazard levels (as opposed to the largest predictable event), can achieve a selected performance objective [2]. Performance-based engineering approaches are frequently adopted for large structures and infrastructures, for which a pre-scribed level of safety or a serviceability state level must be guaranteed. The overall concept of performance-based engineering provides an attractive alternative for owners, since it enables cost-effective design, reduces planning in the aftermath of a catastrophic event and avoids expensive repairs of the system consequent to exceedance of a limit state. Structural optimization under uncertainties has recently gained importance in many engineering fields such as aerospace, aeronautics, infrastructural engineering [2,3] and more recently in wind engineering [4,5]. Randomness in the design variables is an important issue for the performance-based engineering approach, also because uncertainty can regard various design variables [6]. In wind engineering spectral-based and peak-estimation methods have been recognized since the early stages of the research activities on high-rise building response (e.g., [7–10]) due to the presence of random turbulence in the structural loading and dynamic vibration. Nevertheless, the concept of performance-based engineering still deserves careful consideration.

Researchers recently proposed several optimization methods for wind-excited structures, considering uncertainty in structural parameters and wind loads [11–13] and uncertainties in the mass distribution [12,14]. Among wind sensitive structures, self-supporting towers present specific design problems, related to the definition of wind load and the dynamic properties of the structure (e.g. monopole towers [15,16], wind turbine towers [17–19]).

Uncertainties can arise from errors in wind tunnel test, modeling simplifications or as a result of unanticipated modifications of some structural characteristics during structural lifetime [6]. Moreover, the problem of icing can introduce uncertainties in the definition of both dead and wind loads [20].

It is generally recognized that flexible structures, such as communication towers or masts utilized for meteorological measurements, are very sensitive to wind effects and to uncertainties related to wind load and structural dynamic characteristics [6,14]. For these reasons, the optimal design of these structures cannot disregard the importance of parameter uncertainties [16] with a focus on structural performance.

Generally, uncertainties can be grouped into two sets of variables (e.g. [6]); the first set includes structural parameters such as mass, stiffness and the size of structural elements; the second set characterizes

* Corresponding author at: Department of Civil and Environmental Engineering, 400 Snell Engineering Center, Northeastern University, 360 Huntington Avenue, Boston, MA 02115, USA.
E-mail address: lucac@coe.neu.edu (L. Caracoglia).

https://doi.org/10.1016/j.engstruct.2018.07.081
Received 7 April 2018; Received in revised form 15 June 2018; Accepted 25 July 2018

Nomenclature

Abbreviations

BF	"brute force" (Monte-Carlo sampling)
DOF	degree of freedom
FORM	first-order reliability method
LSAMC	layered stochastic approximation Monte-Carlo
SA	stochastic approximation
SGA	stochastic gradient approximation

Symbols and variables

A	projected area of communication devices installed on monopole tower
a_k	gain parameter at step k (Stochastic Approximation)
a	arbitrary constant of the gain parameter (Stochastic Approximation)
C	arbitrary constant of the gain parameter (Stochastic Approximation)
C_D	simulated drag coefficient (stochastic variable)
$C_{D,i}$	*i-th*e element of the simulated drag coefficient sequence (stochastic variable)
E	modulus of elasticity of the material (mast cross section)
F_T	structural response fragility
f	natural frequency [Hz]
f_{01}	fundamental-mode natural frequency of the monopole tower [Hz]
g	peak response factor
h	monopole tower height
$H(f)$	normalized mechanical admittance function for point-like structure (Davenport Chain [50])
I	moment of inertia of area of the reference cross section of the tower mast
$M_{\text{base},0}$	overturning moment at the base of the monopole tower, limit-state threshold
m	simulated mass of the tower (lumped mass, stochastic variable)
m_j	j-th element of simulated mass m sequence (stochastic variable)
N	number equally-probable sets (LSAMC approach)
n	number of samples (Monte Carlo sampling)
P	probability of exceedance
$P_{E,AA}$	probability of exceedance found by approximate approach (FORM or LSAMC)
$P_{E,BF}$	probability of exceedance found by Monte-Carlo sampling (BF)
p	generic stochastic variable p (FORM)
S_{uu}	along-wind horizontal turbulence velocity spectrum
t_0	reference duration of the observation for peak estimation
$\overline{U}$	mean wind speed at $z = h$ (tower top)
$\overline{U}_M$	average value of the mean-wind speed corresponding to structural response threshold crossing (MC approach)
$\overline{U}_M^*$	average value of the mean-wind speed corresponding to structural response threshold crossing (LSAMC approach)
V_z	mean wind velocity at $z = h$ (tower top)
X_{peak}	random variable (peak lateral displacement)
$\overline{x}$	mean along-wind displacement at $z = h$ (tower top)
x_0	peak lateral displacement threshold for the predefined limit state at $z = h$ (tower top)
x_{peak}	peak lateral displacement at $z = h$ (tower top)
z	elevation or vertical coordinate along the vertical axis of the tower
δ	arbitrary constant of the gain parameter (Stochastic Approximation)
$\Lambda_{r,CD}$	r-th subset of simulated drag coefficient (stochastic variable)
$\Lambda_{s,m}$	s-th subset of simulated mass (stochastic variable)
$\upsilon_{0,x}^+$	arrival rate of up-crossings of the peak value (Davenport Chain [50])
ξ_1	generalized response variable (first lateral mode)
ρ	air density
$\sigma_{\xi 1}$	along-wind RMS response corresponding to generalized response ξ_1
$\Upsilon(\overline{U})$	threshold function Eq. (4) (Stochastic Approximation)
$\Phi_1(z)$	normalized lateral first-mode shape of the tower/mast
$\chi(f)$	aerodynamic admittance function for point-like structure (Davenport Chain [50])

Subscripts and superscripts

k	index of k-th iteration step of SA algorithm (Eq. (5))
r	index of r-th equally probable set of drag coefficient ($\Lambda_{r,CD}$)
s	index of *s-th* equally probable set of mass ($\Lambda_{s,m}$)

the dynamic load acting on the structure such as wind, wind speed, turbulence spectra, tributary or projected areas of the loads and aerodynamic force coefficients.

In the present work, the along-wind response of a generalized model of a monopole tower is employed as a first prototype application. This structure is examined, without any loss of generality, as a point-like structure; a generalized single Degree-Of-Freedom (DOF) model is utilized to simulate the dynamic behavior of the considered monopole tower. Two random variables are selected as representative examples of the two fundamental problems, introduced above and usually associated with the analysis of the structural performance via structural fragility functions (e.g. [21,22]): experimental errors in the aerodynamic wind loads and insufficient knowledge of the structural system. The two selected variables are, respectively, the aerodynamic drag coefficient of the tower elements and the mass of the structure [6,12]. Even though other sources of uncertainty are possible (e.g. structural damping, etc. [23–25]), the two quantities above are employed as illustrative indicators for verification of the proposed method along with the benchmark structural model.

Following recent advances in wind engineering of long-span bridges and tall buildings [22,26,27], performance-based structural analysis is accomplished through construction of fragility functions. These are usually assembled as the probability of exceeding a pre-selected limit-state threshold, conditional on the value of mean wind speed at a reference elevation (e.g. [21,22]). The Monte Carlo approach is conveniently employed for structural analysis and commonly applied for the fragility analysis of wind-sensitive structures (e.g. [21,28]). In the present paper a Layered Stochastic-Approximation-Monte-Carlo (LSAMC) approach, based on implementation of the Stochastic Approximation (SA) is proposed [29,30] to accomplish this task. The LSAMC approach enables the statistical assessment of the wind-induced response in presence of "uncertain scenarios". The LSAMC approach is a viable alternative to a standard Monte Carlo simulation ("brute force method"; e.g. [31]), which requires the generation of a large and statistically meaningful number of realizations of the stochastic problem to determine the response to wind load.

Originally conceived as a tool for statistical computation, the SA has been widely used in electrical engineering, subsequently extended to study the non-linear dynamics of cable networks in cable-stayed bridges [32,33] and the dynamic performance of tall buildings subjected to

turbulent wind loads [29,34]. After briefly reviewing the main problem and the SA fundamentals, this paper examines a novel implementation of the SA to compute the higher-order statistical moments of the peak random structural dynamic response in presence of "two-variable uncertainty", related to both wind loading and modeling simplifications. For example, computation of higher statistical moments is needed if the input random variables (namely the aerodynamic loads [21,35,36]) are represented through non-standard probability distribution models (e.g. gamma distribution) and, consequently, the fragility analysis of the output structural response either requires evaluation of the skewness coefficient or a distribution model that differs from the one commonly employed in the practice (e.g. log-normal).

The main objective of this study is the formulation of the LSAMC approach in wind engineering and its verification through application to the dynamics of a monopole tower accounting for the two sources of uncertainty defined above. The accuracy and efficiency of the algorithm, in terms of computing time, are investigated through systematic comparison against more computationally expensive Monte-Carlo sampling methods (e.g. [31,37]) and another popular method, used for structural reliability, i.e. the first-order reliability method (FORM, e.g. [38,39]). Needless to say, other methods have been proposed for the reliability analysis of wind-sensitive structures, such as Markov-Chain Monte Carlo simulation methods (e.g. for offshore wind turbine design [40]), subset simulation methods [41], response surface methods [42]. Nevertheless, the comparison and verification is restricted to the FORM since it is widely employed in the wind engineering field (for example in long-span bridge aerodynamics [43,44]) and can easily be adapted to the numerical estimation of structural fragility curves (as later demonstrated in this study).

The article is organized as follows. In Section 2 a brief background on dynamic response under turbulent loads is presented. In Sections 3 and 4 the LSAMC methodology is illustrated. Section 5 briefly introduces the use of Monte-Carlo sampling methods and the derivation of the FORM in relation to the estimation of structural fragility functions. Section 6 contains the numerical verification of the proposed algorithm, the numerical fragility results and the comparisons against the FORM. The conclusions are summarized in Section 7.

2. Background: dynamic response under turbulent wind loads

The proposed methodology utilizes standard frequency-domain random-vibration analysis for the estimation of wind-induced loading and dynamic response on a slender vertical structure. The procedure assumes that the dynamic behavior of the monopole structure under consideration is linear-elastic. The approach is employed to analyze the dynamic response at large wind velocities, for which buffeting response is the main concern. The aerodynamic loading is based on equivalent quasi-steady formulation of wind forces [8,10,45]. Mean direction of the incident wind is considered horizontal and orthogonal to the principal lateral plane of structural deformation. The wind force is concentrated on the top of the structure where a lumped mass m is used to simulate the weight of the monopole tower; distributed loads along the vertical shaft are neglected. Load induced by vortex shedding is also neglected in this preliminary investigation, since aeroelastic effects due to vortex shedding are primarily important at lower wind speeds, and are usually less critical for displacements as opposed to accelerations [10,46]. Other aeroelastic instabilities are not considered in the present formulation. Fig. 1 is a schematic depicting both the prototype application and the structural mode with axis orientation, concentrated wind loading $F_d(t)$, and lateral bending displacements as a result of the dynamic response; displacements are considered continuous along the cantilever structure, $x(z, t)$, and simulated through the product of a first-mode generalized model [dimensionless mode shape $\Phi_1(z)$, normalized to 1 at $z = h$] and a generalized time-dependent coordinate $\xi_1(t)$ (coincident with the tower-top lateral displacement at $z = h$).

The first-mode generalized model of the structure, considered herein as a prototype of a monopole tower, essentially consists of one dynamic degree of freedom, where the quantities m and A are respectively used to simulate the lumped mass and the projected area of the communication devices which are the main source of mass (weight) and wind loads. The main properties of the structure are summarized in Table 1. It is noted that several authors have used a similar formulation, i.e., a generalized equivalent SDOF model, accounting for first-mode vibration only to describe the structural response of lighting support structures, masts and utility poles [23–25].

Even though the distributed mass of the mast and aerodynamic forces acting on the mast are neglected at this stage, the same approach can be readily extended to a more detailed structural system. Since the main objective of this study is the characterization, verification and first implementation of the LSAMC approach, more complete applications will be considered in future studies.

The wind loads are simulated by exclusively considering the along-wind (drag) forces acting on the communication devices, located at the top of the tower. The loads account for both the wind pressure effect associated with both horizontal mean wind speed ($\overline{U}$) and along-wind horizontal turbulence component (u) at the elevation of the communicating devices ($z = h$). The turbulent component of the wind velocity is modeled as a zero-mean stationary random process, whose probabilistic properties are completely defined by its power spectral density function [$S_{uu}(f)$]. In the present study the power spectrum proposed by Kaimal [47] is employed. The conversion from turbulence spectrum to wind load spectrum utilizes the Davenport approach for point-like structures [48,49] (i.e., the "Davenport chain", [50]). This approach includes derivation of aerodynamic admittance function $\chi(f)$ and mechanical admittance function $H(f)$ (with f frequency in Hz), and subsequent evaluation of the peak response through peak-factor analysis [50].

The standard deviation and the spectrum [$S_{uu}(f)$] of the turbulent component of the wind velocity at $z = h$ are obtained from wind load information derived from the Eurocode 1 standard for exposure terrain category II [51].

The main equations for the evaluation of dynamic response of the system in the along-wind direction can be summarized as follows (e.g., [49]):

$$\sigma_{\xi 1}^2 = \int_0^\infty S_{\xi 1 \xi 1}(f)df = \frac{(\rho C_D A U)^2}{m^2 (2\pi f_{01})^4} \int_0^\infty |H(f)|^2 |\chi(f)|^2 (f) S_{uu} \mathrm{d}f \tag{1}$$

$$x_{peak} = \overline{x} + g\sigma_{\xi 1} \tag{2}$$

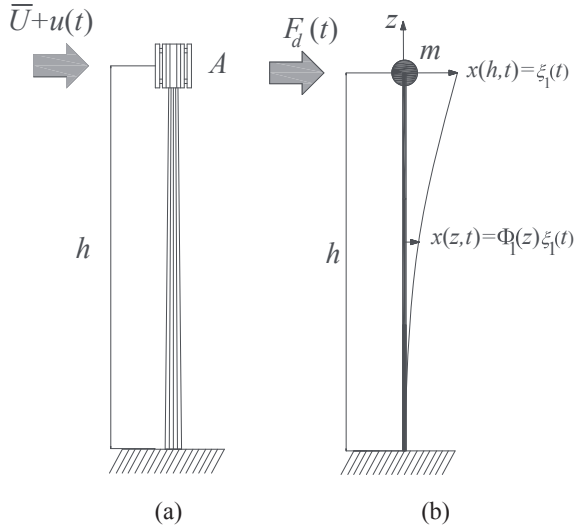

Fig. 1. Monopole tower: (a) Schematic of the structure, (b) generalized model, orientation, loading and displacements.

Table 1
Main properties of the monopole structure.

Structural or geometrical property	Units	Value assigned
Lumped mass m	[kg]	600
Total reference height h	[m]	35.0
Moment of inertia I	[m^4]	2.04×10^{-2}
Modulus of elasticity E	[MPa]	2.00×10^5
Projected area A	[m^2]	8.0
Fundamental-mode structural frequency	[Hz]	0.7
Structural damping ratio	[–]	0.02

$$g = \sqrt{2\ln(\upsilon_{0,x}^{+} t_0)} + \frac{0.577}{\sqrt{2\ln(\upsilon_{0,x}^{+} t_0)}} \tag{3}$$

In Eq. (1) the variance of the lateral along-wind generalized response $\xi_1(t)$ is found from the integration along the frequency axis f [Hz] of the combined complex aerodynamic admittance and mechanical admittance functions. The response depends on the aerodynamic load through the C_D drag coefficient, the lumped mass m of the tower point-like structural model, the fundamental-mode natural frequency f_{01} and the air density ρ; Eq. (2) provides, through the peak coefficient g [Eq. (3)], the peak displacement x_{peak} of the monopole tower top at $z = h$; t_0 is the reference duration of the observation (equivalent to averaging time of wind speed, 10 min) and $\upsilon_{0,x}^{+}$ is the up-crossing rate of the given response threshold (equal to the rate of zero crossings for a narrow band process, in accordance with Davenport's theory, [49]). The Davenport chain and its relationship to wind-induced response and uncertainty analysis are presented in Fig. 2.

3. Formulation of the LSAMC approach

This chapter discusses the fundamentals of the LSAMC approach and its algorithmic implementation. In the present paper, the algorithm has been employed to statistically derive the along-wind stochastic dynamic response of a prototype monopole tower, modeled as a generalized system (first-mode response).

Table 2
Mean values and coefficient of variation of the uncertain model parameters.

Statistical moments	C_D [–]	m [kg]
Mean value	1.20	600
Coefficient of variation	0.42	0.17

Without any loss of generality, the proposed methodology has been applied to an SDOF dynamic problem with uncertainties in the wind loading and in the structural properties. Uncertain parameters are the drag coefficient C_D and the lumped mass m, which respectively simulate the effect of variable shapes and weight of the communication devices [14,53]. In the present work, the lognormal distribution model is used to describe the two uncertain parameters; the two random parameters are uncorrelated [6]. Previous studies [6,21,29] indicated that the number of random samples n must be adequately chosen to examine the empirical probability distribution of the output variable x_{peak}, and to evaluate its mean and standard deviation. Contrary to standard application of the Davenport Chain, the peak value becomes a random variable because of the random C_D and m; mean values and coefficient of variation of the uncertain model parameters were calibrated using literature results (e.g., [21]). Numerical values are described in Table 2.

3.1. Brute force approach

The stochastic response of the considered system can be examined by repeatedly solving Eqs. (1)-(3) assuming a random sequence of drag coefficient values $\{C_{D,1}, C_{D,2}, ..., C_{D,n}\}$ and mass values $\{m_1, m_2, ..., m_n\}$. To apply the SA approach, combined with Monte Carlo sampling, it is useful to re-define the problem of x_{peak} exceeding a pre-selected

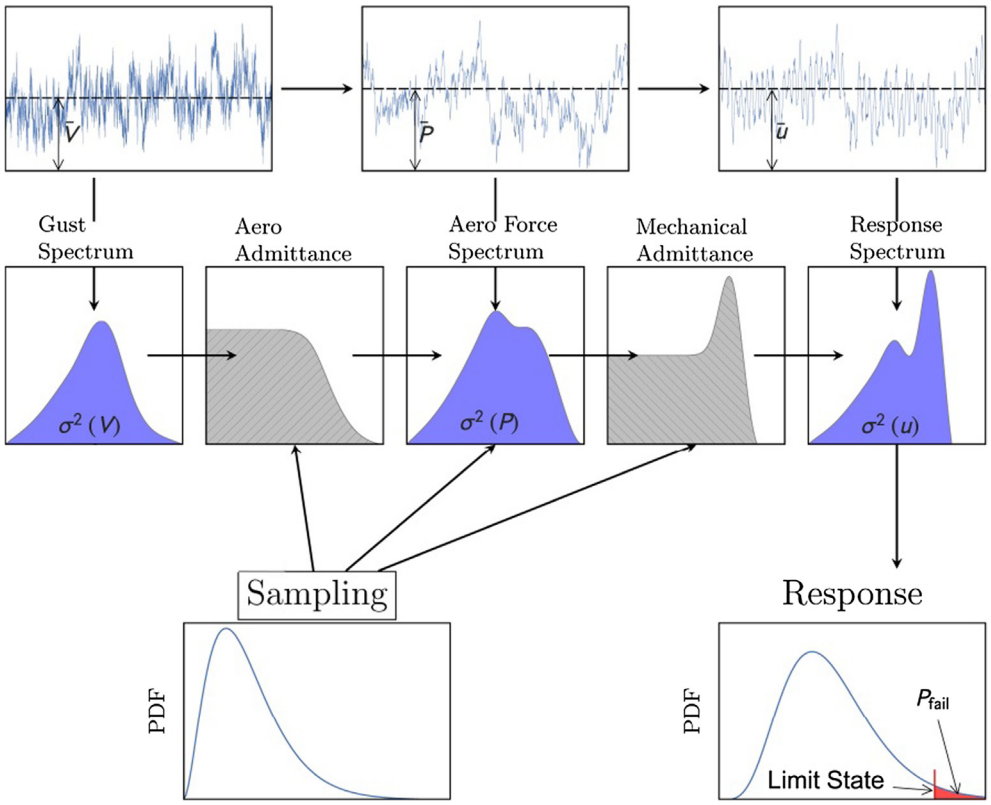

Fig. 2. Davenport Chain and its relationship to wind-induced response and uncertainty analysis.
Image reproduced from [52].

threshold x_0. The function below is defined:

$$\Upsilon_k(\overline{U}_k, C_{D,k}, m_k) = [\overline{x}(\overline{U}_k, C_{D,k}, m_k) + g\sigma_{\xi 1}(\overline{U}_k, C_{D,k}, m_k)] - x_0. \quad (4)$$

In the previous equation Υ_k is a function that depends on Eq. (2), which has been appropriately rewritten as function of the random variables C_D and m. This equation implies that the gust effect factor g remains approximately constant despite the randomness in the mass m and C_D; $\upsilon^+_{0,x}$ (Eq. (3)) is approximately constant if the overall shape of the response spectrum (i.e., the integral in Eq. (1)) does not considerably change with the randomness in the variables C_D and m. The present approximation is acceptable in the context of this exploratory study. Furthermore, it may be further relaxed in the implementation of the LSAMC approach but it was not discussed herein also to enable the comparison against other probability-based methods (e.g. FORM), later presented in the paper. In any case, it can be considered in future studies.

The roots of this equation correspond to the crossing of the threshold x_0, i.e. the mean wind speed at the monopole tower top $\overline{U}_k$ that yields $\Upsilon_k = 0$ for a given value of $C_{D,k}$ and m_k. This equation must be numerically solved for each k-th value of the n samples to find the roots.

Once a threshold related to the limit state x_0 is selected, Eq. (4) with $k = 1, ..., n$ leads to the sequence corresponding to the first-threshold crossings values of the mean-wind speed $\{\overline{U}_1, \overline{U}_2, ..., \overline{U}_n\}$, at which the predefined limit state is reached. It must be noted that the lateral displacement limit state at the monopole top (i.e., the threshold x_0) can be easily replaced by the corresponding bending moment acting at the base of the monopole through the relationship $M_{base,0} = 3EIh^{-2}x_0$, where E is the elastic modulus of the mast cross section and I the moment of inertia of area.

3.2. Stochastic approximation algorithm (estimation of the mean wind speed $\overline{U}^*_M$)

Originally conceived as a tool for statistical computations, the SA has been widely used in engineering. The areas of "adaptive signal processing" in communication engineering and of control engineering have extensively employed the SA algorithms. A similar algorithm, called stochastic gradient approximation (SGA), has been introduced for optimization problems in Variational Quantum Monte Carlo Many-Body Physics [54]. In the present work the SA is used to find the stochastic response under preselected "uncertain scenarios", which simulate the presence of structural uncertainties, modeling simplifications and aerodynamic load variability.

According to the Robbins-Monro Theorem [55,56] and to previous works performed by the authors [30,57], an approximate value $\overline{U}^*_M$ of the true average value $\overline{U}^*_M$ (average of the mean wind speed at threshold crossing) related to the sequence $\{\overline{U}_1, \overline{U}_2, ..., \overline{U}_n\}$ can be found recursively, at the k-th step, as follows:

$$\overline{U}^*_{M,k+1} = \overline{U}^*_{M,k} - a_k \Upsilon_k(\overline{U}^*_{M,k}, C_{D,k}, m_k), \quad (5)$$

where $\overline{U}^*_{M,k}$ represents the independent variable (mean wind speed [m/s]) of the function Υ_k, which is needed to find the root [m] (Eq. (4)), and a_k is the damping term [1/s] utilized for the convergence of the procedure.

The SA simple recursive formula estimates the average of the mean wind speed at first crossing of x_0 at the k-th step, $\overline{U}^*_{M,k}$, from the random sequence of drag coefficients $C_{D,k}$ and mass distribution m_k. At each k-th iteration, the recursive procedure selects $C_{D,k}$ and m_k randomly from the distributions of the sampled random variables [30,57] without solving for $\Upsilon_k = 0$ at each step. The recursive procedure stops when the variation of the solution is below a predefined tolerance, assuming $\overline{U}^*_{M,k} = \overline{U}^*_{M,k+1}$. Eq. (5) uses a "damping term" a_k that satisfies the Robbins-Monro condition [56].

$$\sum_{k=1}^{\infty} a_k^2 < \infty \text{ and } \sum_{k=1}^{\infty} a_k = \infty. \quad (6)$$

A possible solution for a_k can be written as [55]

$$a_k = \frac{a}{(k + 1 + C)^{\delta}}, \quad (7)$$

where $0.5 < \delta < 2.0$, a and C are arbitrary constants that are chosen to accelerate the numerical convergence. Previous studies [33,57] have suggested that, in standard conditions and for the problem analyzed herein, the values $\delta = 0.51$, $a = 10$ and $C = 0$ are good choices for convergence of the method.

Figs. 3–5 illustrate, as a proof-of-concept, the application of the SA. The procedure examines three cases: C_D random and deterministic mass m, deterministic C_D and m random, both C_D and m are random variables. Inspection of Figs. 3–5 reveals that the SA tends to an approximate value of $\overline{U}^*_M$; it also shows a direct comparison between the approximate value $\overline{U}^*_M$, obtained by SA, and the "exact" value of $\overline{U}^*_M$, which is obtained by Monte Carlo sampling since evaluation of a closed-form solution is usually impractical.

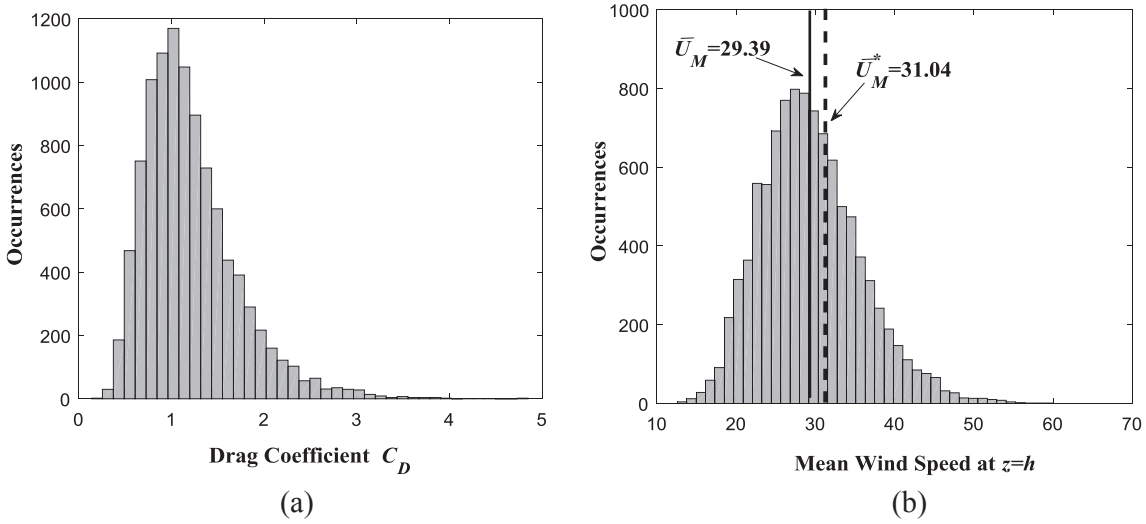

Fig. 3. (a) Empirical distribution of uncertain drag coefficient C_D (n = 10, 000) of the monopole structure with deterministic mass m = 600 kg; (b) sequence of first-threshold-crossing mean-wind speed for the limit state corresponding to x_0 = 0.70 m.

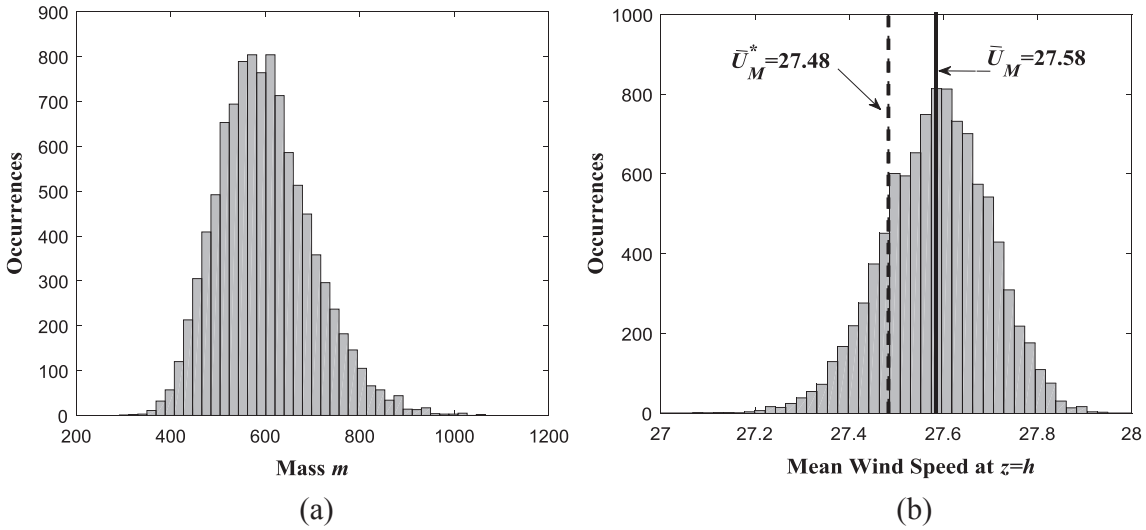

Fig. 4. (a) Empirical distribution of uncertain mass m (n = 10, 000 as an example) of the monopole structure with deterministic drag coefficient C_D = 1.2; (b) sequence of the first-threshold-crossing mean-wind speeds for the limit state corresponding to x_0 = 0.70 m.

3.3. Description of the LSAMC approach

According to Eq. (4), the analysis of the along-wind response exceeding a predefined limit state provides the corresponding sequence of mean wind speeds $\{\overline{U}_k\}$ for threshold crossing, based on the random sequences $\{C_{D,k}\}$ and $\{m_k\}$.

The LSAMC approach extends the standard SA algorithm, described in the previous section, and estimates, in a computationally efficient way, mean and higher statistical moments of the sequence $\{\overline{U}_k\}$.

The approach considers a layered sampling from the sequences of the continuous random variables $\{C_{D,k}\}$ and $\{m_k\}$, forming a finite number of sub-sets Λ_{r,C_D} and $\Lambda_{s,m}$, respectively identified by indices r and s. Each sub-set is based on a subdivision of the original set into adjacent non-overlapping equally-probable sets (i.e., the intervals toward the tail of the distribution are larger in extension compared to the ones near the mean value of the distribution). The continuous random variables over each sub-set can be replaced by a discrete random variable with given probability mass function, centered at the mean value for each set. For example, $C_{D,k} \in \Lambda_{r,C_D}$ and $m_k \in \Lambda_{s,m}$ are sampled from the N by N equal-probability independent intervals or "sets", with $r = 1, \ldots, N$ and $s = 1, \ldots, N$. The following equations must be satisfied:

$$\bigcup_r \Lambda_{r,C_D} = \{C_D\} \text{ and } \bigcap_r \Lambda_{r,C_D} = \varnothing, \tag{8}$$

$$\bigcup_s \Lambda_{s,m} = \{m\} \text{ and } \bigcap_s \Lambda_{s,m} = \varnothing. \tag{9}$$

The standard SA is independently applied to each sub-set, and the average of the mean-wind speed corresponding to the crossing of the threshold x_0 is found as $(\overline{U}^*_{M,k+1})_{(\Lambda_{r,C_D},\Lambda_{s,m})}$ using Eq. (5). The subscript in the variable $(\overline{U}^*_{M,k+1})_{(\Lambda_{r,C_D},\Lambda_{s,m})}$ pertains to the index associated with a generic set Λ_{r,C_D} and $\Lambda_{s,m}$. This proposition yields:

$$(\overline{U}^*_{M,k+1})_{(\Lambda_{r,C_D},\Lambda_{s,m})} = (\overline{U}^*_{M,k})_{(\Lambda_{r,C_D},\Lambda_{s,m})} - a_k \Upsilon_k[(\overline{U}^*_{M,k})_{(\Lambda_{r,C_D},\Lambda_{s,m})}, (C_{D,k})_{(\Lambda_{r,C_D})}, (m_k)_{(\Lambda_{s,m})}]. \tag{10}$$

The recursive Eq. (10), applied separately in each Λ_{r,C_D} and $\Lambda_{s,m}$ set, converges to a representative discrete point which is the local expected value of $\overline{U}^*_{M,r,s}$; the notation is simplified and Λ_{r,C_D} and $\Lambda_{s,m}$ are simply denoted by their indices r and s. Consequently, the SA is applied N by N times, "layering" the sampling to each Λ_{r,C_D} and $\Lambda_{s,m}$; this procedure is similar to the Latin Hypercube sampling often employed for better

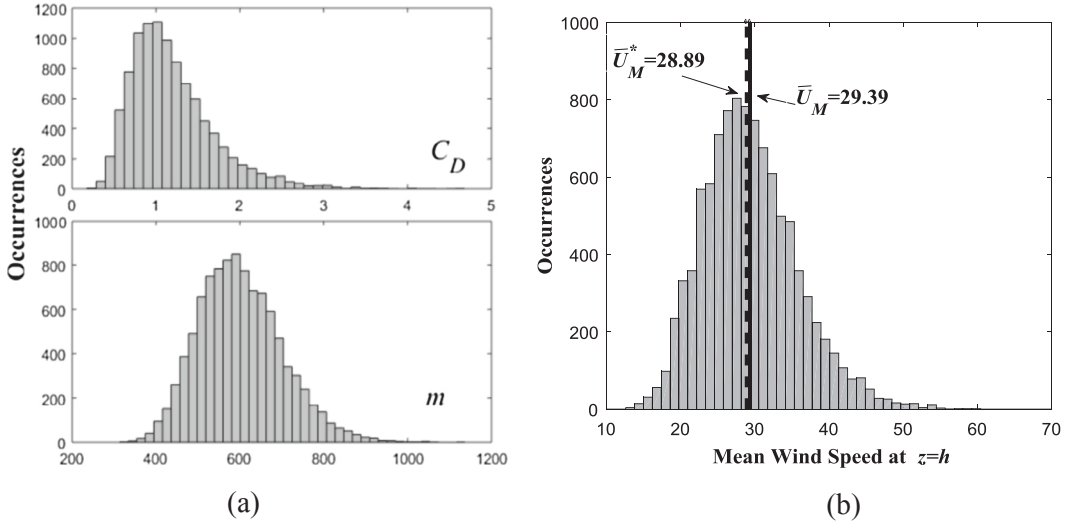

Fig. 5. (a) Empirical distributions of uncertain parameters C_D and m (n = 10, 000 as an example); (b) sequence of first-threshold-crossing mean-wind speed for the limit state corresponding to x_0 = 0.70 m.

convergence of the Monte Carlo method [31,37].

In the case of a single uncertain variable (e.g., random C_D and deterministic mass m), the proposed approach is applied with probability mass function PMF = $1/N$ [30] to approximate the mean, standard deviation (SD) and skewness (SK) coefficient of the continuous target random variable $\overline{U}$ at first crossing of the threshold x_0:

$$\mathrm{E}_{\overline{U}} \approx \overline{U}^*_M = \sum_{r=1}^{N} (\overline{U}^*_{M,r} \cdot \mathrm{PMF}), \tag{11}$$

$$\mathrm{SD}_{\overline{U}} \approx \left[\sum_{r=1}^{N} ((\overline{U}^*_{M,r} - \overline{U}^*_M) \cdot \mathrm{PMF}) \right]^{0.5}, \tag{12}$$

$$\mathrm{SK}_{\overline{U}} \approx \frac{\sum_{r=1}^{N} ((\overline{U}^*_{M,r} - \overline{U}^*_M)^3 \cdot \mathrm{PMF})}{[SD(\overline{U})]^3}. \tag{13}$$

Although the skewness coefficient is not directly needed if the log-normal model is employed for fragility curve estimation, this additional moment can be useful in case that other distribution models are employed. Furthermore, the evaluation of Eq. (13) is useful for the verification of the numerical approach and, consequently, it is included in the numerical simulations of Section 4.

Fig. 6 illustrates, as a proof-of-concept, application of the LSAMC to the present case. The algorithm converges to an approximate value of $\overline{U}^*_M$, standard deviation (SD) and skewness coefficient (SK) are also indicated; the total number of realizations is 10,000, according to Eqs. (11)-(13) for $N = 4$ equally-probable sets, designated by variables $C_{D,k} \in \Lambda_{r,C_D}$ with $r = 1, \ldots, N$ and constant mass m. The four areas, delimited by the vertical dashed lines and enclosed by the empirical distribution bins in Fig. 6, are the same.

The SA algorithm has been separately applied to each r-th set, Λ_{r,C_D}, with the random variable $C_{D,k} \in \Lambda_{r,C_D}$ corresponding to the data markers with red dots in Fig. 6a. The algorithm converges to an approximate value $\overline{U}^*_M$ of the "exact" mean speed $\overline{U}_M$, obtained by Monte Carlo sampling; the equivalent discrete points are indicated by red-dot markers in Fig. 6b.

In presence of two uncertain parameters (C_D and m), mean, standard deviation and skewness continuous target random variable $\overline{U}$ at first crossing of the threshold x_0 are evaluated, with probability mass function PMF = $1/N^2$, as:

$$\mathrm{E}_{\overline{U}} \approx \overline{U}^*_M = \sum_{r=1}^{N} \sum_{s=1}^{N} (\overline{U}^*_{M,r,s} \cdot \mathrm{PMF}), \tag{14}$$

$$\mathrm{SD}_{\overline{U}} \approx \left[\sum_{r=1}^{N} \sum_{s=1}^{N} ((\overline{U}^*_{M,r,s} - \overline{U}^*_M)^2 \cdot \mathrm{PMF}) \right]^{0.5}, \tag{15}$$

$$\mathrm{SK}_{\overline{U}} \approx \frac{\sum_{r=1}^{N} \sum_{s=1}^{N} ((\overline{U}^*_{M,r,s} - \overline{U}^*_M)^3 \cdot \mathrm{PMF})}{[SD(\overline{U})]^3}. \tag{16}$$

The same approach illustrated in Fig. 6, can be readily extended to the case of two-variable uncertainty, where the stochastic variables are C_D and m. In this second case, the SA algorithm can separately be applied to each r-th set, Λ_{r,C_D}, and s-th set, $\Lambda_{s,m}$, with the random variables $C_{D,k} \in \Lambda_{r,C_D}$, $m_k \in \Lambda_{s,m}$ and with r and s varying between 1 and N.

Fig. 7 illustrates a second application of the LSAMC algorithm in the case of two uncertain parameters. The procedure is applied to assess an approximate value of mean, standard deviation and skewness of $\overline{U}$ with random variables C_D and m; the total number of realizations (n) is 10,000. According to Eqs. (14)-(16) the procedure employs a layering that comprises $N \times N = 4 \times 4$ equally-probable sets, designated as Λ_{r,C_D} with $r = 1, \ldots, N$ and $\Lambda_{s,m}$ with $s = 1, \ldots, N$.

4. Verification of the layered LSAMC algorithm

Verification of the LSAMC algorithm is illustrated in this section. Comparison between LSAMC (approximate) and Monte Carlo (BF) reference solutions is carried out. We examine the mean, standard deviation and skewness of the random mean-wind speed $\overline{U}$, which is related to the dynamic response of the monopole structure crossing the threshold x_0. Figs. 8–10 illustrate various verification examples with both one uncertain input random variable and two uncertain input random variables.

The sensitivity of the "exact" solution by Monte Carlo simulation (BF) is also studied by varying the sample size n; each Monte Carlo simulation is also repeated twenty times. Figs. 8–10 present the scatter plots with the results of the 20 consecutive Monte Carlo simulations (small-size markers), as a function of the sample size $n \in \{500,\ 5000,\ 10,000,\ 15,000\}$.

The figures also show the approximated values of the mean, standard deviation and skewness of $\overline{U}$ obtained by LSAMC (large-size markers), as a function of the number of the subsets

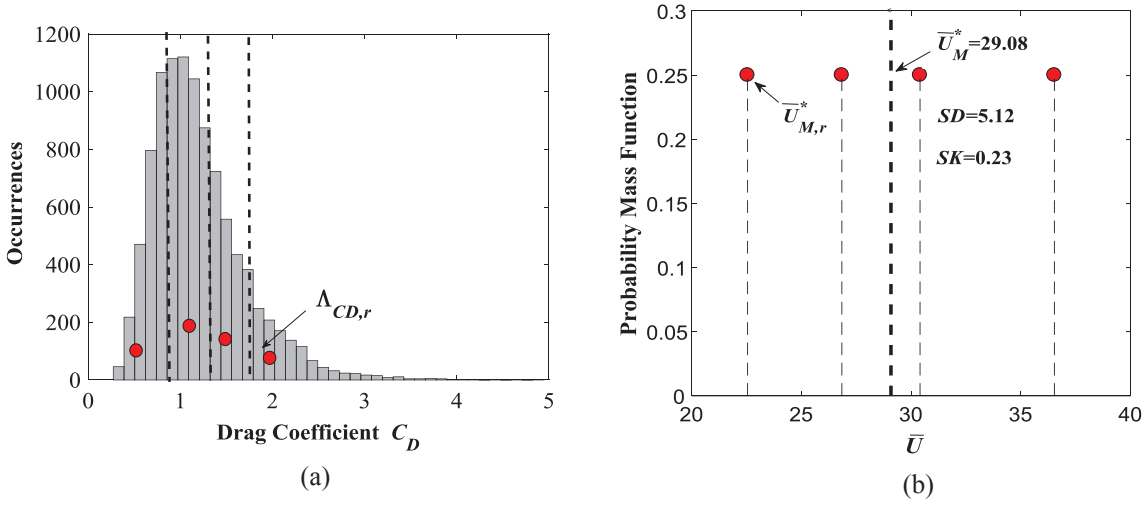

Fig. 6. Random estimations of the mean-wind speed $\overline{U}$ (at $z = h$), relative to the response limit state corresponding to threshold crossing $x_0 = 0.70$ m with random drag coefficient:(a) empirical histogram of the random input C_D with indication of the "layered sub-sets" Λ_{r,C_D} ($N = 4$; note: equally-probable sub-sets are schematically illustrated), (b) PMF of the output discrete $\overline{U}^*_{M,r}$ derived by LSAMC (mean value $\overline{U}^*_M$, standard deviation, SD, and skewness, SK, computed from the discrete $\overline{U}^*_{M,r}$ points are also indicated).

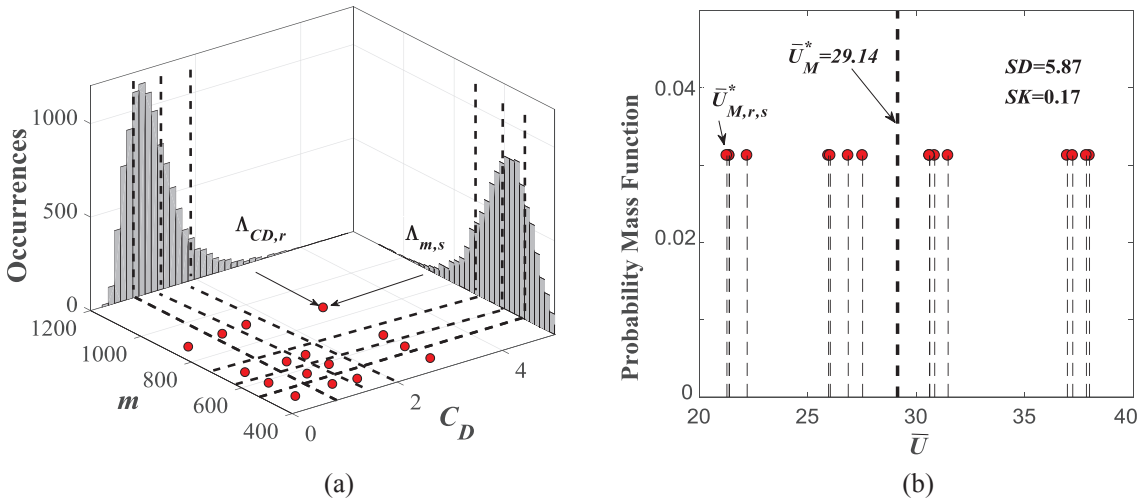

Fig. 7. Random estimations of the mean-wind speed $\bar{U}$ (at $z = h$), relative to the response limit state corresponding to threshold crossing $x_0 = 0.70$ m with both random drag coefficient and mass: (a) empirical histograms of the random input C_D and m with indication of the "layered sub-sets" Λ_{r,C_D} and $\Lambda_{s,m}$ ($N \times N = 4 \times 4$; note: equally-probable sub-sets are schematically illustrated), (b) PMF of the output discrete $\bar{U}^*_{M,r,s}$ derived by LSAMC (mean value $\bar{U}^*_M$, standard deviation, SD, and skewness, SK, computed from the discrete $\bar{U}^*_{M,r,s}$ points are also indicated).

$N \in \{10,\ 20,\ 40,\ 60\}$. The results in Fig. 8 are presented for the three cases of: random C_D and deterministic mass m (Fig. 8a); deterministic C_D and random mass m (Fig. 8b) and both C_D and m random (Fig. 8c). Inspection of the results reveals that the LSAMC method provides a very precise estimation of the mean value for $N = 20$ sub-sets (equally-probable sets) in the case of one input random variable (e.g., for $N = 20$ the relative error between LSAMC and BF is less than 0.2% in Fig. 8a and b); in the case of two random variables (Fig. 8c) the same precision of the LSAMC requires a larger number of sub-sets $N \times N = 10 \times 10 = 100$.

Furthermore, as can be seen from Fig. 8, the precision increases with the number of sets N.

Fig. 9 shows the comparisons between the two approaches related to the estimation of the standard deviation of $\bar{U}$, which is connected to the dynamic response of the monopole structure crossing the threshold x_0.

Initial examination of Fig. 9 suggests that a good approximation of the SD is achieved at $N = 20$ (error less than 2%) in the case of one input random variable (Fig. 9a and b), and $N \times N = 20 \times 20 = 400$ with two input random variables. Even in this second scenario, the precision of the LSAMC increases with the increment of the number of subsets (Fig. 8).

It is also noted in Fig. 9b that, despite the small SD values, the LSAMC achieves a very precise approximation with a relative small number of sub-sets (e.g., with $N = 20$ the relative error of SD estimation is less than 3%); this remark proves that the LSAMC algorithm can be considered a reliable approach even in the case that the estimated quantity has of small magnitude.

Fig. 10 suggests that the LSAMC algorithm is apparently less accurate in estimating the skewness coefficient of $\bar{U}$. The normalized error is about 10% with one input random variable (Fig. 10a and b) and $N = 60$; in case of two random variables, the number of sub-sets needed to achieve the same precision becomes $N \times N = 60 \times 60 = 1200$. The "exact" value of the skewness of $\bar{U}$, suggested by Monte Carlo sampling, is in fact very small. This leads to larger relative errors of the LSAMC estimators, around 15%. Nevertheless, the SK estimation by LSAMC method is adequate, despite seemingly larger errors, as it can still preserve sufficient information on the probability distribution of the random $\bar{U}$ for fragility analysis. It will be demonstrated in the subsequent section that the relative errors in case of a fragility analysis are smaller and that the LSMAC is quite accurate. It is also observed that the small discrepancies, noted for the skewness values obtained by the LSAMC, do not affect the fragility results later shown in this paper.

The same procedure described in this section was extended to other threshold levels x_0; results are similar but are not shown for the sake of brevity. Information on mean and standard deviation of $\bar{U}$ will be employed in the next section to evaluate the structural fragility curves, directly by LSAMC.

The results, shown in Figs. 8–10, confirm the high potentialities of the proposed LSAMC algorithm, which allows determining very precise approximations of mean and standard deviation of $\bar{U}$ with a very small number of subsets. Moreover, examination of Figs. 8–10 suggests that the standard Monte Carlo method needs a much higher number of samples n to achieve good estimations of the same quantities since the procedure needs to solve for the roots of Eq. (4) for all repetitions.

Table 3 shows the comparison of the normalized computing times needed to obtain the results shown in Figs. 8–10 by Monte Carlo sampling and LSAMC approach for various sample sizes n. Numerical efficiency of the LSAMC approach is evident from the data shown in the table.

5. Fragility analysis by stochastic methods: theoretical background

Fragility analysis has been recently examined for performance-based structural analysis against wind hazards [58–61]. The objective of a fragility analysis is the computation of the conditional probability of exceedance of representative limit states through the assessment of indicators (designated as "engineering demand parameters"), which correspond to a specific feature of the dynamic response. Examples are: the maximum lateral drift of the tower, the internal bending moments or shear forces in the generic section. A set of thresholds is usually defined to represent different levels of structural performance, based on such indicators, which may be selected by the designer.

Complementary cumulative distributions functions (CCDF) are used to derive the structural fragility (F_T), i.e., to find the probability that the generic random variable x_{peak}(e.g., peak response of monopole tower top) exceeds a preselected threshold T, conditional on the presence of a wind storm with mean speed $V_z = \bar{U}$ at the reference height $z = h$, as

$$F_T(V_z) = \text{Prob}[X_{peak} > T | V_z = \bar{U}]. \tag{17}$$

In the derivation of Eq. (17) the effect of random variables simulating uncertainty in the wind load estimation and modeling errors (i.e., random variables C_D and m in the specific application) can readily be included.

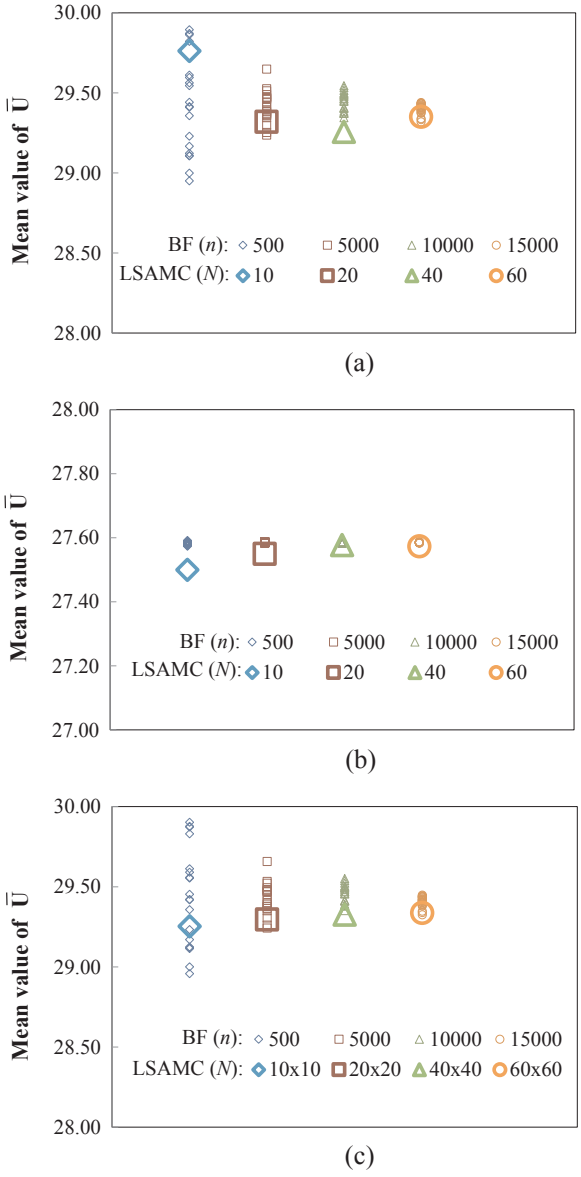

Fig. 8. Comparison between expected value of $\overline{U}$, found by Monte Carlo method (Brute Force, BF) for various sample sizes n, and approximated averages obtained by LSAMC with different N subsets: (a) random C_D and constant mass m, (b) constant C_D and random m, (c) both C_D and m random variables.

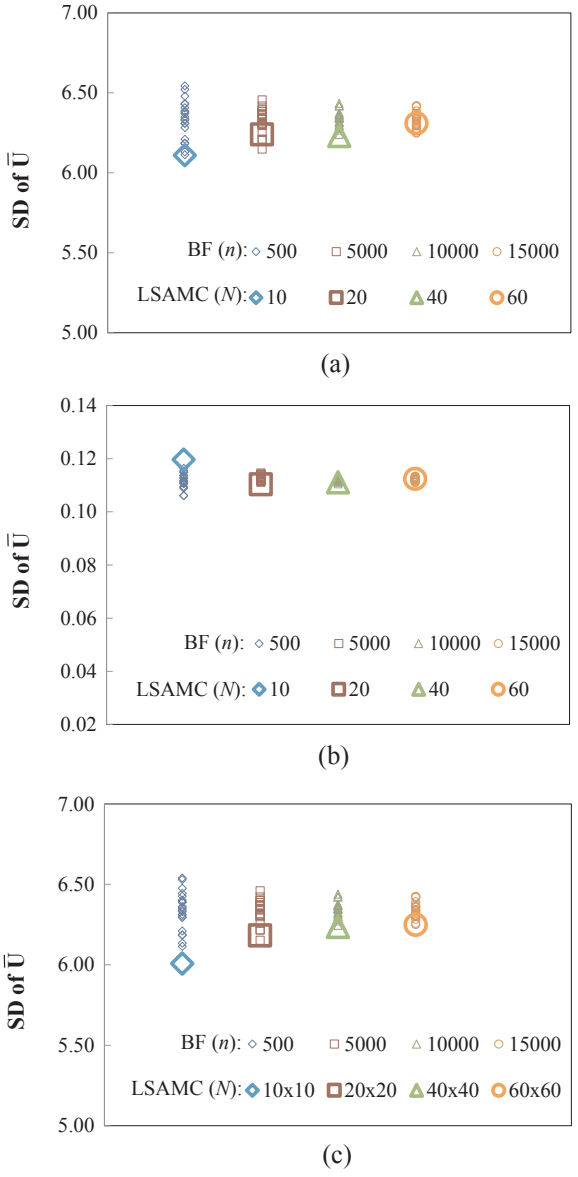

Fig. 9. Comparison between standard deviations (SD) of $\overline{U}$, found by Monte Carlo method (Brute Force, BF) at various sample sizes n, and approximated SD values obtained by LSAMC with different N subsets: (a) random C_D and constant mass m, (b) constant C_D and random m, (c) both C_D and m random variables.

5.1. Fragility functions via Monte-Carlo sampling (Brute force approach)

Traditionally, fragility curves are numerically estimated through Monte Carlo sampling [21,22], for example utilizing Eq. (2) to empirically estimate the peak response (random variable X_{peak} in equation above) and compare it against threshold T through sampling. This approach is usually preferred by researchers due to its accuracy and robustness. Nevertheless, large computing time is usually needed and represents the "bottle-neck" of this method. Details are omitted in this study for the sake of brevity but examples may be found in previous studies (e.g. [21,22]).

5.2. Fragility functions via LSAMC approach

The LSAMC approach, presented above, can also be employed for the fragility analysis of wind-sensitive monopole towers. The LSAMC algorithm allows determining the mean and standard deviation of $\overline{U}$, mean wind speed associated with peak lateral response that corresponds to the first crossing of the threshold x_0. The quantity $\overline{U}$ is a random variable, as shown in the previous sections. Information about mean and statistical moments of the random $\overline{U}$ can be used to construct the curves in Eq. (17), noting that $V_z = \overline{U}$ and using the cumulative distribution function of $\overline{U}$ to approximate the structural fragility curve. Preliminary investigation is necessary to determine the distribution model that best describes the random $\overline{U}$ which is needed to postulate the model of the fragility function.

5.3. Fragility functions via implementation of perturbation methods (FORM)

In the case of a uni-variate random property, such as C_D and m, the quantity x_{peak} (Eq. (2)) becomes a random variable. Estimation of the probability density function of x_{peak}, affected by random C_D and m, can be approximated through perturbation methods. Implementation of the

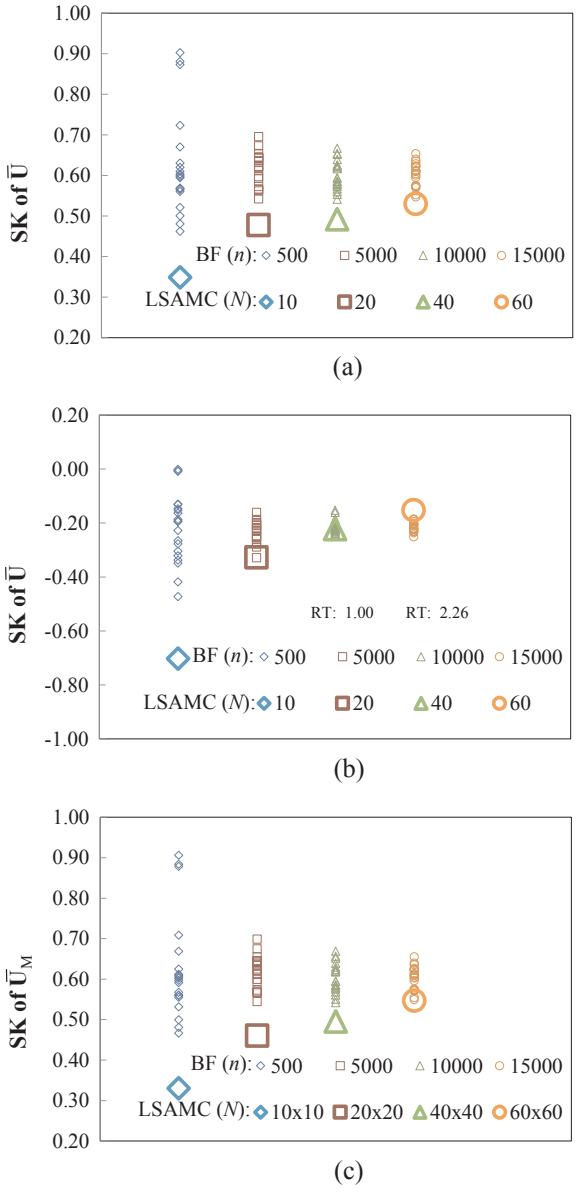

Fig. 10. Comparison between skewness coefficients (SK) of $\bar{U}$, found by Monte Carlo method (Brute Force, BF) at various sample sizes n, and approximated SK values obtained by LSAMC with different N subsets: (a) random C_D and constant mass m, (b) constant C_D and random m, (c) both C_D and m random variables.

FORM [38,39] can be used for this purpose, along with the functional relationship between x_{peak} and the input random properties (C_D and m), evaluated at each $\bar{U}$.

The treatment is based on the single-input single-output functional relationship between input random property (either C_D or m) and x_{peak}. Extension to multiple random-variable input is readily available but is not presented herein. Derivations are briefly summarized in this subsection.

It must be noted that implementation of the FORM is considered in a non-conventional setting, contrary to standard reliability engineering applications [38,39]. The perturbation method is in fact employed to approximate the functional relationship between input random property and x_{peak}. Consequently, the FORM is used to only indirectly examine the limit-state probability that x_{peak} exceeds the threshold x_0, conditional on the value of $\bar{U}$ [i.e., structural fragility functions; Eq. (17)].

Since x_{peak} depends on both mean response $\bar{x}$ and the fluctuations

Table 3
Examination of normalized computing times needed to estimate mean, standard deviation and skewness (refer to the results in Figs. 8–10; computing time is related to each single operation, shown by a marker in the figures, and normalized to BF time with two random variables and sample size n = 10, 000).

BF		LSAMC	
Sample size n (BF)	Computing time	Subsets N (LSAMC)	Computing time
C_D (Fig. 8)			
500	0.0473	10	0.0002
5000	0.4794	20	0.0005
10,000	0.9452	40	0.0010
15,000	1.3927	60	0.0015
m (Fig. 9)			
500	0.0464	10	0.0002
5000	0.4886	20	0.0005
10,000	0.9498	40	0.0010
15,000	1.3790	60	0.0013
C_D and m (Fig. 10)			
500	0.0476	10 × 10	0.0022
5000	0.4977	20 × 20	0.0092
10,000	1.0000	40 × 40	0.0399
15,000	1.4429	60 × 60	0.0880

σ_{ξ_1}, the perturbation approach must be applied twice to independently determine two relationships (for $\bar{x}$ and σ_{ξ_1}) and the input random property (either C_D or m). Moreover, as previously outlined, the gust effect factor g varies slowly with stochasticity and it is assumed constant, independent of randomness.

Denoting the generic input stochastic variable p (to designate either C_D or m) the two functions $\bar{x}$ and σ_{ξ_1} are expressed by Taylor series about a "reference design point" and truncated to the first order of the expansion. This reference point is determined using the mean input value $\bar{p}$, i.e. in the absence of input randomness. This expansion is illustrated in Eqs. (18) and (19):

$$\bar{x}(p) \approx \bar{x}(\bar{p}) + \left[\left.\frac{d\bar{x}}{dg}\right|_{p=\bar{p}}\right](p-\bar{p}) = y_0(\bar{p}) + \left[\left.\frac{dy_0}{dg}\right|_{p=\bar{p}}\right](p-\bar{p}), \tag{18}$$

$$\sigma_{\xi_1}(p) \approx \sigma_{\xi_1}(\bar{p}) + \left[\left.\frac{d\sigma_{\xi_1}}{dp}\right|_{p=\bar{p}}\right](p-\bar{p}) = y_1(\bar{p}) + \left[\left.\frac{dy_1}{dg}\right|_{p=\bar{p}}\right](p-\bar{p}). \tag{19}$$

In the previous expressions the quantities y_0 and y_1 designate the nonlinear functional relationship between either $\bar{x}$ or σ_{ξ_1} and generic input random variable p, i.e. $\bar{x} = y_0(p)$ and $\sigma_{\xi_1} = y_1(p)$, evaluated in the proximity of the reference design point ($p = \bar{p}$). From the definition of peak response (Eq. (2)) and the hypothesis of constant g (Eq. (3)), the mean, mean square value and the variance (VAR) of x_{peak} can be evaluated, using the reference design point $p = \bar{p} = \mathrm{E}[p]$, as:

$$\mathrm{E}[x_{peak}] = \bar{x}(\bar{p}) + g\sigma_{\xi_1}(\bar{p}) = \bar{y}_0(\bar{p}) + gy_1(\bar{p}), \tag{20}$$

$$\mathrm{E}[x_{peak}^2] \approx \mathrm{E}[(\bar{x} + g\sigma_{\xi_1})^2] = \mathrm{E}[\bar{x}^2] + \mathrm{E}[\sigma_{\xi_1}^2]g^2 + 2g\mathrm{E}[\bar{x}\sigma_{\xi_1}], \tag{21}$$

$$\mathrm{VAR}[x_{peak}] \approx \mathrm{E}[x_{peak}^2] - (\mathrm{E}[x_{peak}])^2; \tag{22}$$

where the symbol E[.] designates expectation operator. To approximately derive the probability distribution of x_{peak}, the mean value and the standard deviation (or the variance, VAR) of x_{peak} are needed. The former quantity is directly derived from Eq. (20) above, whereas the latter requires the estimation of the second statistical moments $\mathrm{E}[\bar{x}^2]$, $\mathrm{E}[\sigma_{\xi_1}^2]$ and $\mathrm{E}[\bar{x}\sigma_{\xi_1}]$. These quantities are also approximately found by FORM as:

$$\mathrm{E}[\overline{x}^2] \approx \mathrm{E}[y_0^2(\overline{p})] + \left[\left.\frac{\mathrm{d}y_0}{\mathrm{d}p}\right|_{p=\overline{p}}\right]^2 \mathrm{E}[(p-\overline{p})^2], \tag{23}$$

$$\mathrm{E}[\sigma_{\xi 1}^2] \approx \mathrm{E}[y_1^2(\overline{p})] + \left[\left.\frac{\mathrm{d}y_1}{\mathrm{d}p}\right|_{p=\overline{p}}\right]^2 \mathrm{E}[(p-\overline{p})^2], \tag{24}$$

$$\mathrm{E}[\overline{x}\sigma_{\xi 1}] \approx \mathrm{E}[y_0(\overline{p})y_1(\overline{p})] + \mathrm{E}[(p-\overline{p})^2]\left[\left.\frac{\mathrm{d}y_0}{\mathrm{d}p}\right|_{p=\overline{p}}\right]\left[\left.\frac{\mathrm{d}y_1}{\mathrm{d}p}\right|_{p=\overline{p}}\right]. \tag{25}$$

In deriving Eq. (25) the relationship $\mathrm{E}[p-\overline{p}]=0$ is used; the derivatives of y_0 and y_1 with respect to p are evaluated at the reference design point. After rewriting the variance term as $\mathrm{E}[(p-\overline{p})^2] = \mathrm{VAR}[p]$ and combining Eqs. (23)-(25) with Eqs. (21) and (22) the variance of the peak response, $\mathrm{VAR}[x_{peak}]$, becomes:

$$\mathrm{VAR}[x_{peak}] \approx \mathrm{VAR}[p]\left\{\left(\left.\frac{\mathrm{d}y_0}{\mathrm{d}p}\right|_{p=\overline{p}}\right)^2 + 2g\left(\left.\frac{\mathrm{d}y_0}{\mathrm{d}p}\right|_{p=\overline{p}}\right)\left(\left.\frac{\mathrm{d}y_1}{\mathrm{d}p}\right|_{p=\overline{p}}\right) + g^2\left(\left.\frac{\mathrm{d}y_1}{\mathrm{d}p}\right|_{p=\overline{p}}\right)^2\right\}. \tag{26}$$

Eqs. (20) and (26) can be used to find an expression for the probability distribution function of x_{peak} at each wind speed $\overline{U}$, using $\overline{p} = \mathrm{E}[p]$ and $\mathrm{VAR}[p]$; the probability model describing the response variable x_{peak} is in fact the same as the one of the input random variable p owing to the approximate linear relationship established by FORM. This information can be employed to re-construct the cumulative distribution function of x_{peak} at each $\overline{U}$ and, consequently the complementary cumulative distribution function dictated by the fragility relationship ((Eq. (17)), after the threshold level x_0 is chosen. Since the relationships y_0 and y_1 cannot typically be found in closed form, numerical estimation of the derivatives in Eq. (26) is found by sampling these functions in the proximity of $p = \overline{p} = \mathrm{E}[p]$.

6. Structural fragility analysis: Results and comparisons (LSAMC, FORM and BF)

6.1. Computation of structural fragility functions with one input random property (either C_D or m)

This sub-section examines the structural fragility analysis of the single-DOF generalized model of the prototype monopole tower under the influence of both wind loading (C_D variable) and structural property uncertainties (mass m). As described earlier, randomization of these parameters reflects the presence of either measurement errors in the wind tunnel or structural uncertainties related to the modification of the structural mode shape or structural mass during the lifetime.

The main purpose is to evaluate the effectiveness of the LSAMC approach. The comparisons of the fragility curves include the various methods (Monte Carlo sampling, LSAMC approach and FORM). In this investigation, fragility curves are evaluated by computation of the probability that the along-wind peak dynamic response at $z = h$ exceeds a pre-selected threshold x_0, corresponding to the limit state of the peak lateral displacement at the monopole tower top.

For the Monte-Carlo simulations, the number of samples $n = 10,000$ has been considered as the reference value. From the verification results of the LSAMC approach, presented in the previous section, it is suggested that the lognormal model can be used to replicate the cumulative distribution function of $\overline{U}$ and, consequently, the fragility function.

Table 4 summarizes the predefined threshold levels, utilized for the fragility analysis $x_0 \in \{T1, T2, T3, T4, T5\}$. Threshold T5 is related to a possibly unrealistic peak displacement, but is utilized herein mainly for verification of the proposed procedure. Table 4 also presents the corresponding base bending moment thresholds M_0, derived from x_0 and the properties of the monopole structure; this second quantity can be used to examine the ultimate limit state either associated with either maximum overturning moment of the tower or material strength in the base cross section.

The main results are presented in Figs. 11 and 12. Fig. 11 shows the fragility curves calculated for random C_D (random aerodynamic loads) and deterministic mass $m = 600$ kg. Fig. 12 similarly depicts the fragility curves for deterministic aerodynamic load (C_D) and random mass m. In both Figs. 11 and 12 the graphs found with Monte-Carlo sampling (Brute Force, BF) are used as the reference solution; the left panels of both figures present the comparisons with the LSAMC whereas the right sides illustrate the results found with the FORM.

Comparison of Fig. 9(a) with (b) indicates that the standard deviation of the random $\overline{U}$ is larger in the case of a C_D random variable and becomes almost negligible in the case of deterministic C_D and random mass m. This observation is also confirmed by examination of the fragility curves shown in Fig. 12, where a small variation of the wind speed $\overline{U}$ induces an abrupt performance loss; the steep slope locally exhibited by the fragility curves is indeed an indicator of limited sensitivity to randomness.

Overall, as anticipated by the small errors found with the LSAMC in Figs. 8 and 9, the agreement of the approximated LSAMC estimations with the "exact" curves, found by Monte-Carlo sampling, is very good in both Figs. 11 and 12. The FORM is still adequate when uncertainty propagation considers the random C_D (Fig. 11(b)), whereas substantial discrepancies are observed in Fig. 12(b) with random mass m. From a cursory analysis of the results shown in Figs. 11 and 12, it is noted that LSAMC provides a good approximation of fragility curves with relative small differences (or errors). Estimation errors can be qualitatively noticed by inspection of the fragility curves.

The LSAMC approach is usually adequate, in particular when small variability in the random input property or parameter leads to "step-like" fragility functions in Fig. 12(a). On the contrary, the FORM is unable to replicate the structural fragility in Fig. 11(b). The estimation error of the LSAMC, approximately evaluated by inspection of the fragility curves, is about few percent. A quantitative examination of the error is presented in the next sub-section.

6.2. Analysis of simulation errors with one input random property (either C_D or m)

The relative estimation error provided by the two approximated approaches (AA) is defined as $(P_{E,AA}-P_{E,BF})/P_{E,BF}$, where $P_{E,AA}$ and $P_{E,BF}$ respectively designate probability of exceedance obtained by approximate solution (LSAMC or FORM) and "exact" probability of exceedance obtained by Monte-Carlo sampling (Brute Force, BF). Estimation error calculations are carried out by comparing the graphs in Figs. 11 and 12 at several values of $\overline{U}$; results are illustrated in Fig. 13 for random drag coefficient C_D and Fig. 14 for random mass m. In each case, the left panels present the SLAMC results while the right panels the FORM ones, enabling cross-examination of the two methods.

In Fig. 13, the error of the LSAMC is larger at low wind speeds $\overline{U}$ and decrease to about 4% for wind speeds greater than 40 m/s; the FORM gives considerably larger errors for all considered wind velocities. In

Table 4
Thresholds for fragility analysis of the generalized model of the monopole structure.

Threshold level x_0	Tower top displacement threshold level [m]	Base bending moment threshold level [kN m]
T1	$0.010h = 0.35$	3488
T2	$0.020h = 0.70$	6977
T3	$0.036h = 1.26$	12, 558
T4	$0.052h = 1.82$	18, 140
T5	$0.068h = 2.38$	23, 722

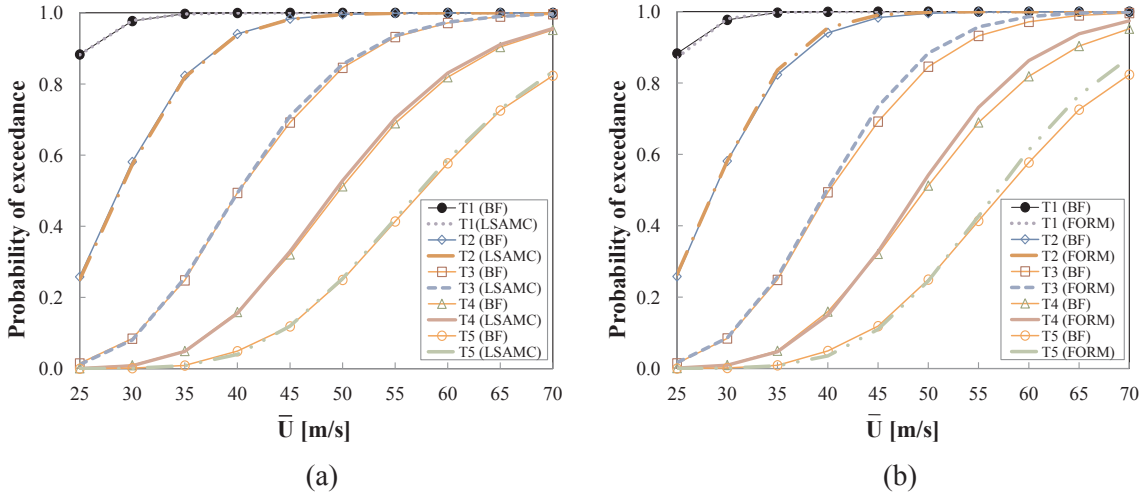

Fig. 11. Fragility curves obtained by Monte-Carlo (BF) sampling, LSAMC and FORM approaches. Analysis of monopole structure with random aerodynamic load (C_D variable) and limit state associated with the lateral peak displacement at $z = h$ and the thresholds T1 – T5 (Table 3): (a) Comparison between Monte Carlo (BF) and LSAMC, (b) Comparison between Monte Carlo (BF) and FORM.

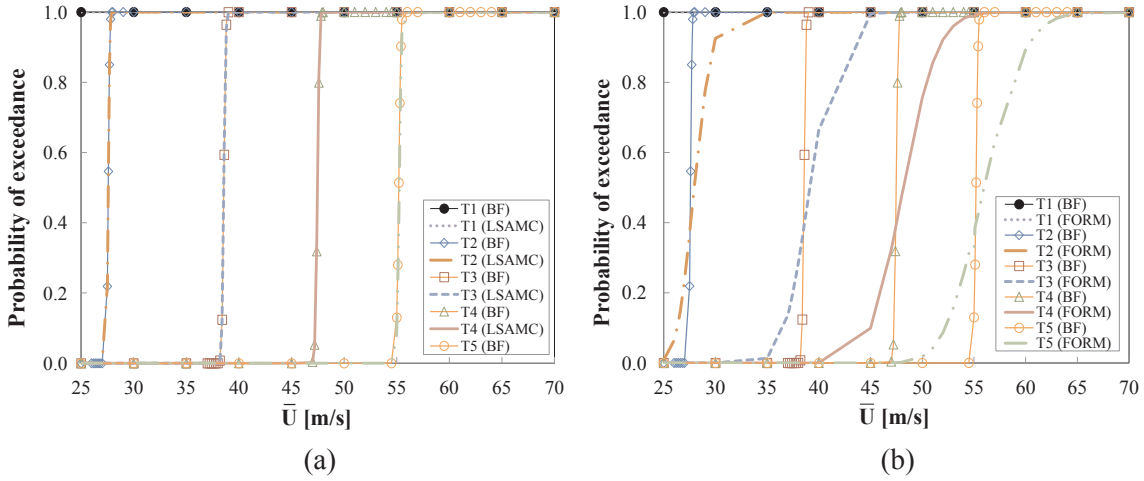

Fig. 12. Fragility curves obtained by Monte-Carlo (BF) sampling, LSAMC and FORM approaches. Analysis of monopole structure with random structural properties (m mass variable) and limit state associated with the lateral peak displacement at $z = h$ and the thresholds T1 – T5 (Table 3): (a) Comparison between Monte Carlo (BF) and LSAMC, (b) Comparison between Monte Carlo (BF) and FORM.

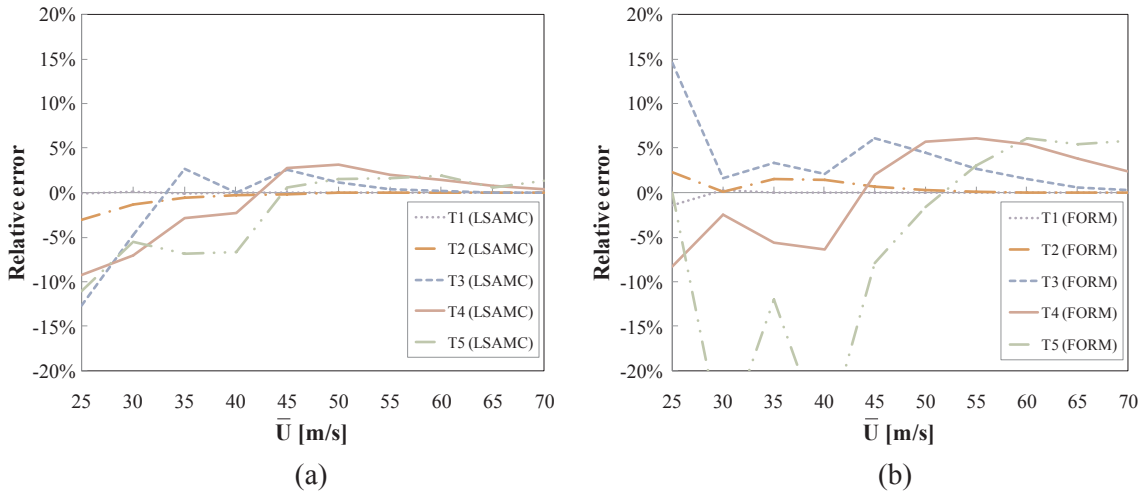

Fig. 13. Relative error of LSAMC and FORM compared to the "exact" solution (Monte Carlo, BF) – C_D random variable and T2, T5 thresholds: (a) Comparison between Monte Carlo (BF) and LSAMC, (b) Comparison between Monte Carlo (BF) and FORM [notes: relative errors shown in the range of wind speeds between 25 m/s and 70 m/s; "60" = number of equiprobable sets].

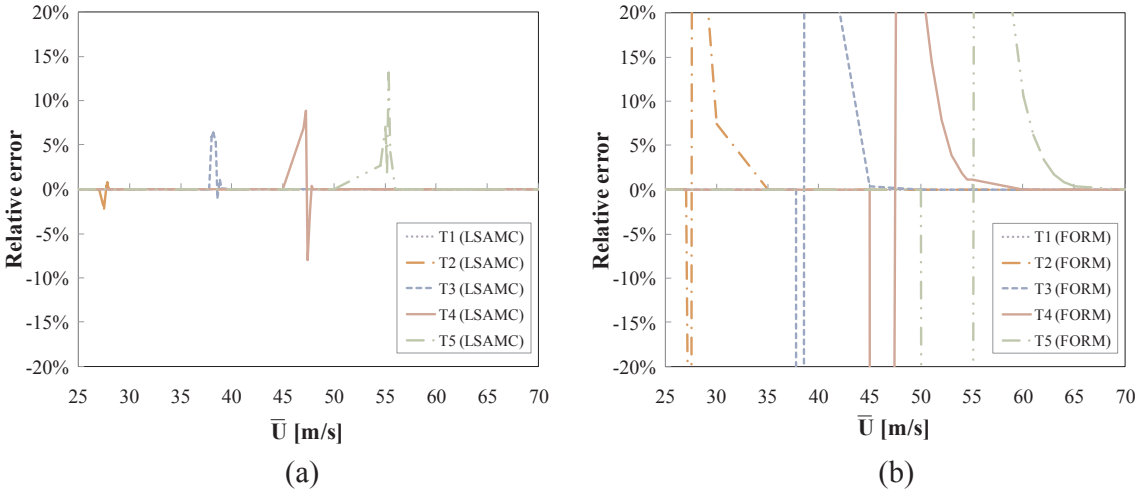

Fig. 14. Relative error of LSAMC and FORM compared to the "exact" solution (Monte Carlo, BF) – m random variable and T2, T5 thresholds: (a) Comparison between Monte Carlo (BF) and LSAM, (b) Comparison between Monte Carlo (BF) and FORM notes: relative errors shown in the range of wind speeds between 25 m/s and 70 m/s; "60" = number of equiprobable sets].

Fig. 14, the discrepancy between Monte-Carlo and approximate solutions is exacerbated by a considerably smaller random variability introduced by the random mass m in the estimation of the x_{peak}. Clearly, the FORM is not adequate as relative errors are very large while the estimation errors associated with the LSAMC approach are still reasonably small. This figure is important since it suggests that, even in the presence of a limiting case associated with small random variability and "steeper" fragility functions for intermediate values of $\overline{U}$ (thus leading to abrupt variations in exceedance probabilities), the LSAMC approach still provides better results compared with FORM.

General examination of Figs. 13 and 14 suggests that the estimation error in the case of LSAMC is localized; fragility curves usually exhibit good agreement with the ones obtained numerically by Monte-Carlo sampling. On the contrary, the error committed by FORM is not acceptable. This problem can be explained accounting for the limitation introduced by the FORM and used for determining the variance of x_{peak}, as illustrated in Eq. (26). Finally, even though verification of the LSAMC procedure has been examined, further validation may be desirable in the future (e.g., through testing and experimental assessment of structural fragility).

6.3. Computation of structural fragility functions with two input random properties (both C_D and m)

Fig. 15(a) presents the structural fragility curves when both C_D and m are the input random properties. This investigation is restricted to the comparison between LSAMC and Monte-Carlo sampling, since the FORM is unable to provide adequate estimation of the fragility curves when the contribution of a random m is incorporated. In this last scenario with two input random variables the relative deviations (errors) between the approximate fragility curves found by LSAMC and the "exact" curves determined by Monte Carlo sampling are illustrated in Fig. 15(b). The relative error, computed as explained in Section 6.2 is slightly smaller than the error found for the first scenario with random C_D only and shown in Fig. 13(a).

The supplementary numerical results illustrated in Fig. 15 confirm the good performance of the LSAMC approach. Qualitative differences between approximate and Monte-Carlo fragility curves (Fig. 15(a)) are almost imperceptible. The relative error between LSAMC and Monte-Carlo sampling is less than 5% for wind speeds $\overline{U}$ larger than 35 m/s.

All the results presented in Figs. 11–15 are preliminary since they are based on the analysis of a generalized structural model of a

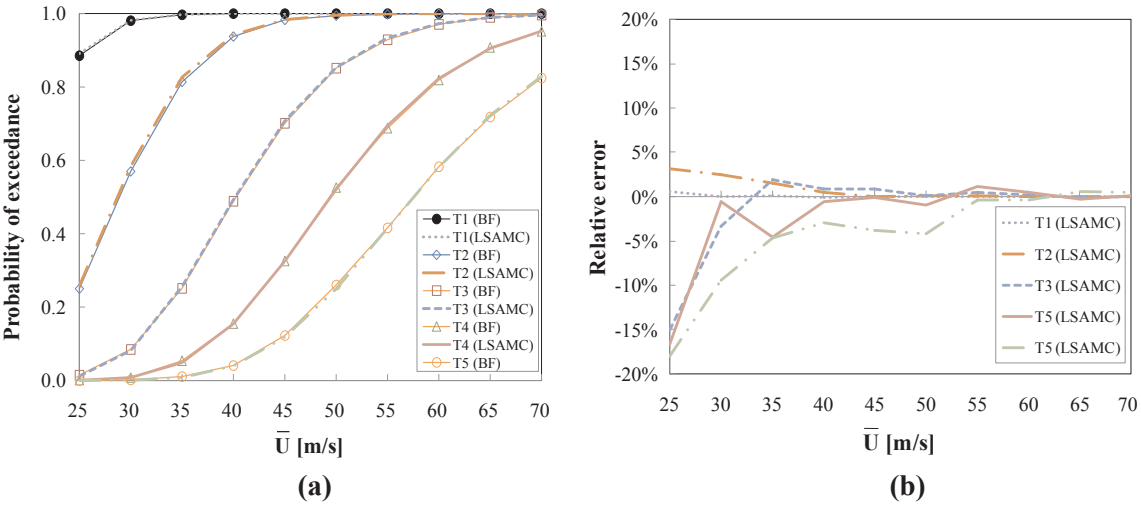

Fig. 15. Fragility curves obtained by Monte-Carlo (BF)sampling and LSAMC approach. Analysis of monopole structure with random structural properties (m mass variable) and random aerodynamic loads (C_D variable) for limit state associated with lateral peak displacement at $z = h$ and thresholds T1 – T5 (Table 3): (a) fragility curves, (b) relative errors [note: relative errors shown between 25 m/s and 70 m/s].

monopole tower. They require further investigation prior to generalization of the LSAMC algorithm and its implementation to other and more complex wind-sensitive vertical structures (tall buildings, wind turbines, etc.). This task is, however, beyond the scope of this study and will be considered in the future.

6.4. Examination of computing time savings

Computational efficiency of the proposed methodology is examined in this sub-section Fig. 16 summarizes the results of this investigation.

The computing time of the LSAMC algorithm is examined as a function of the number of equiprobable sets (N). The execution time is normalized with respect to Monte-Carlo computing (BF-normalized) and compared against the FORM computing time.

The results illustrated in Fig. 16 indicate that, in the case of a single input random variable, the LSAMC achieves sufficient approximation (illustrated in Figs. 11–15) with equiprobable sets $N = 60$ and a BF normalized computing time equal to 0.18%. In Fig. 16(a) and (b) the computing time of LSMAC is modestly longer than the time required by FORM. As expected, in case of two input random variables (Fig. 16(c)) the normalized computing time increases since it is proportional to the number of equiprobable sets needed to obtain the same accuracy, which are 3600 (60×60). Examination of Fig. 16(c) suggests that, in the case of two random variables, the LSAMC algorithm is less performing. Even though the performance of the LSAMC approach may progressively deteriorate as the number of input random variables increase, the LSAMC approach is still 90% faster than Monte-Carlo sampling with two random variables, indicating that it may still be adequate for ordinary applications in performance-based wind engineering.

7. Discussion and conclusions

This study summarizes the results of a research activity aiming at the derivation of computationally-efficient performance-based methodologies for the estimation of structural fragility curves of wind-sensitive structures. Implementation of SA algorithms was employed to derive the dynamic response of a prototype structure, a monopole tower, under stationary wind loads in the frequency domain.

Uncertainty and measurement errors were considered by suitable random perturbation of selected but representative variables (physical properties) of the structure and the load, following implementations presented in previous work [21,22]. The numerical procedure, designated as LSAMC algorithm, was employed to analyze the effects of uncertainty and errors in the modeling of structural properties and in the estimation of wind forces, often carried out in wind tunnel. Linear elastic along-wind dynamic response was considered.

In the first part of the study, initial verification of the LSAMC algorithm was conducted by comparing the simulated results against Monte Carlo sampling results. The comparison was based on the analysis of mean values, variance and skewness coefficients embedded in the implicit stochastic function (Eq. (4)).

In the second part, the LSAMC approach was employed to derive structural fragility curves of the prototype monopole tower, associated with various limit states. The peak lateral response at the top of the tower was employed as the control variable, or engineering demand parameter. Five different limit-state thresholds were considered to assess the stochastic response of the prototype system and evaluate computation of the fragility curves. For the sake of completeness and to identify advantages and potential limitations of the LSAMC, the investigation also examined another popular approach for reliability analysis, the FORM.

Numerical simulations confirm that the LSAMC approach is adequate for approximate estimation of structural fragility curves. The error is usually limited to few percent values. Furthermore, the LSAMC outperforms the FORM when the propagation of uncertainty is either influenced by nonlinearity (mass m) or the steepness in the fragility curves is large (refer to error comparisons in Section 6).

The LSAMC also proves to be an efficient algorithm from the computational point of view, since a significant speedup in the computing time was observed in comparison with Monte-Carlo sampling results (Fig. 16). For example, in the case of single input random property or variable, the computing time required by LSAMC is less than 1% compared to the time needed by Monte-Carlo simulation. In the case of two input random properties or variables, the computing time of LSAMC is about 12% compared to standard sampling approach;

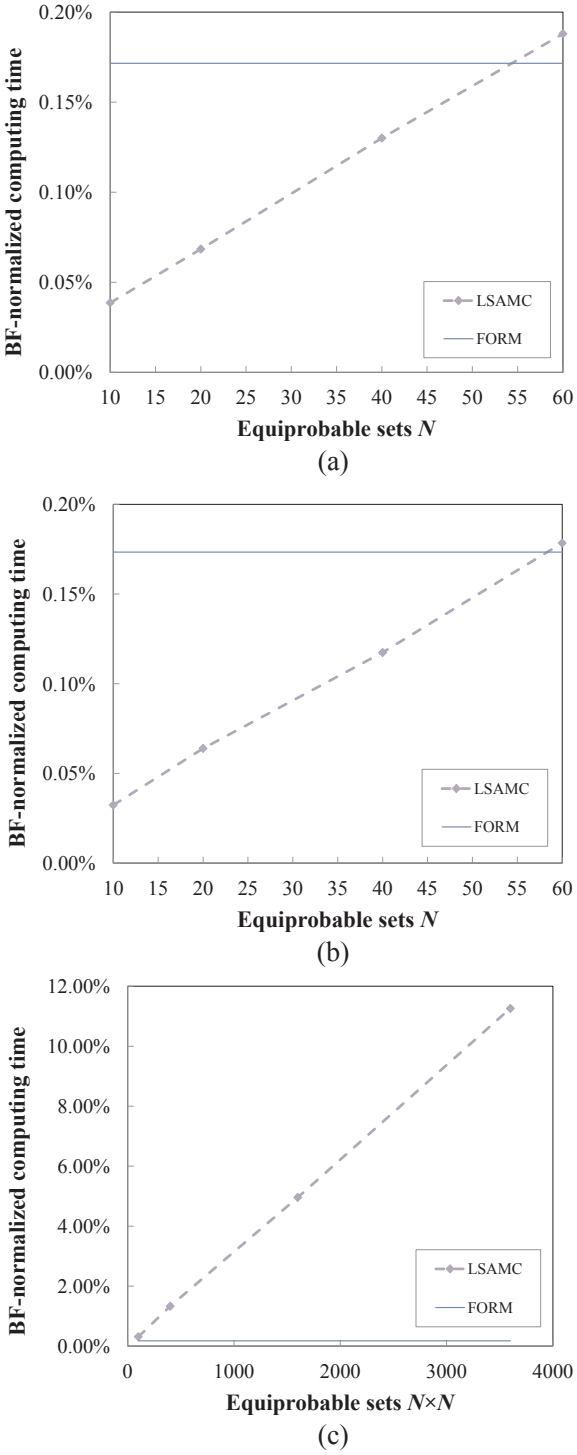

Fig. 16. Computing time of LSAMC and FORM, as a function of the number of equiprobable sets, normalized to the Monte-Carlo (BF) time: (a) random C_D, (b) random m, (c) random C_D and m.

computing time reductions were obtained by preserving adequate accuracy in the approximated structural fragility curves. It is noted that, even though the computing time savings progressively deteriorate when the number of input random variables increase, they appear to be adequate for ordinary applications and conventional structures.

The study primarily examined two types of random behavior, i.e. uncertainty in the aerodynamic loads (simulated through static coefficient C_D) and modeling uncertainty due to imperfect knowledge of the structure (simulate through mass m). Clearly, these two variables are provided as examples, since several other parameters or structural properties (e.g. damping ratios) are perhaps equally relevant [23–25] to the dynamic response. Consequently, more investigation is needed to extend these results to other random variables. Nevertheless, the main objective of the study was the examination of the LSAMC approach as a computationally efficient method for structural fragility analysis.

Future studies should include more complex structural systems, examine other parameter uncertainties, account for across-wind response in addition to along-wind response, and expand the treatment to the stochastic structural analysis in the presence of high-dimensional problems (multi-degree-of-freedom structures).

Acknowledgements

Gian Felice Giaccu acknowledges the financial support of Regione Autonoma della Sardegna, Italy (L.R. n. 3/2008 “RientroCervelli” and L.R. n. 7/2007 “Promozione della Ricerca Scientifica e dell'Innovazione Tecnologica in Sardegna”). The authors would also like to thank Professor Bernardo Barbiellini from the Department of Physics of Lappeenranta University of Technology (Finland) for fruitful discussions about the SA mehods and for providing the original motivation that led to the implementation of the SA algorithm, described in this study.

References

[1] Inokuma A. Basic study of performance-based design in civil engineering; 2002.
[2] Tsompanakis Y, Lagaros ND, Papadrakakis M. Structural design optimization considering uncertainties. London; 2008.
[3] Yao W, Chen X, Luo W, Van Tooren M, Guo J. Review of uncertainty-based multidisciplinary design optimization methods for aerospace vehicles. Prog Aerosp Sci 2011;47:450–79.
[4] Ciampoli M, Petrini F. Performance-based aeolian risk assessment and reduction for tall buildings. Prob Eng Mech 2012;28:75–84.
[5] Ciampoli M, Petrini F, Augusti G. Performance-based wind engineering: towards a general procedure. Struct Saf 2011;32:367–78.
[6] Venanzi I, Materazzi AL, Ierimonti L. Robust and reliable optimization of wind-excited cable stayed masts. J Wind Eng Indust Aerodyn 2015;147:368–79.
[7] Davenport AG. Response of supertall buildings to wind. In: Third international conference on tall buildings. Chicago, IL, United States of America. p. 705–705.
[8] Davenport AG. Response of six building shapes to turbulent wind. Phil Trans R Soc London Ser A 1971;269(1199):385–94.
[9] Kareem A. Dynamic response of high-rise buildings to stochastic wind loads. J Wind Eng Indust Aerodyn 1992;42(1–3):1101–12.
[10] Kareem A. Model for predicting the acrosswind response of buildings. Eng Struct 1984;6(2):136–41.
[11] Spence SMJ, Gioffrè M. Large scale reliability-based design optimization of wind excited tall buildings. Prob Eng Mech 2012;28:206–15.
[12] Spence SMJ, Kareem A. Performance-based design and optimization of uncertain wind-excited dynamic building systems. Eng Struct 2014;78:133–44.
[13] Spence SMJ, Gioffrè M. Efficient algorithms for the reliability optimization of tall buildings. J Wind Eng Indust Aerodyn 2011;99(6–7):691–9.
[14] Venanzi I, Materazzi AL. Robust optimization of a hybrid control system for wind-exposed tall buildings with uncertain mass distribution. Smart Struct Sys 2013;12(6):641–59.
[15] Pavan Kumar M. Effect of wind speed on structural behaviour of Monopole and self-support telecommunication towers. Asian J Civil Eng 2017;18(6):911–27.
[16] Støttrup-Andersen U. Masts and towers. J Int Assoc Shell Spatial Struct 2014;55:79–88.
[17] Dimopoulos CA, Koulatsou K, Petrini F, Gantes CJ. Assessment of stiffening type of the cutout in tubular wind turbine towers under artificial dynamic wind actions. J Comput Nonlin Dyn 2015;10(4). 041004-041004-9.
[18] AlHamaydeha M, Hussain S. Optimized frequency-based foundation design for wind turbine towers utilizing soil–structure interaction. J Franklin I 2011;348(7):1470–87.
[19] Petrini F, Manenti S, Gkoumas K, Bontempi F. Structural design and analysis of offshore wind turbines from a system point of view. Wind Eng 2010;34(1):85–108.
[20] Makkonen L, Lehtonen P, Hirviniemi P. Determining ice loads for tower structure design. Eng Struct 2014;74:224–32.
[21] Smith MA, Caracoglia L. A Monte Carlo based method for the dynamic “fragility analysis” of tall buildings under turbulent wind loading. Eng Struct 2011;33(2):410–20.
[22] Cui W, Caracoglia L. Simulation and analysis of intervention costs due to wind-induced damage on tall building. Eng Struct 2015;87:183–97.
[23] Pagnini L. Reliability analysis of wind-excited structures. J Wind Eng Indust Aerodyn 2010;98(1):1–9.
[24] Pagnini L, Repetto M. The role of parameter uncertainties in the damage prediction of the alongwind-induced fatigue. J Wind Eng Indust Aerodyn 2012;104–106:227–38.
[25] Pagnini L, Solari G. Gust buffeting and turbulence uncertainties. J Wind Eng Indust Aerodyn 2002;90(4):441–59.
[26] Seo D-W, Caracoglia L. Estimating life-cycle monetary losses due to wind hazards: fragility analysis of long-span bridges. Eng Struct 2013;56:1593–606.
[27] Cui W, Caracoglia L. Exploring hurricane wind speed along US Atlantic Coast in warming climate and effects on predictions of structural damage and intervention costs. Eng Struct 2016;112:209–25.
[28] Gao B, Cen D, Wu H. Static performances and reliability sensitivity analysis on rigid cable dome structures. J Shenzhen Univ Sci Eng 2013;30(3):325–30.
[29] Giaccu GF, Scintu L, Barbiellini B. Stochastic approach for the dynamic performance analysis of tall buildings subject to turbulent wind load. In: ICWE14 Conference. Porto Alegre, Brazil; 2015.
[30] Caracoglia L, Giaccu GF, Barbiellini B. Estimating the standard deviation of eigenvalue distributions for the nonlinear free-vibration stochastic dynamics of cable networks. Meccanica 2016:1–15.
[31] Robert CP, Casella G. Monte Carlo statistical methods. 2nd ed. New York, New York, USA: Springer Science; 2004.
[32] Giaccu GF, Barbiellini B, Caracoglia L. Parametric study on the nonlinear dynamics of a three-stay cable network under stochastic free vibration. J Eng Mech, ASCE 2015;141(6):04014166.
[33] Giaccu GF, Barbiellini B, Caracoglia L. Stochastic unilateral free vibration of an in-plane cable network. J Sound Vib 2015;340:95–111.
[34] Scintu L. Approccio stocastico per l'analisi dinamica- prestazionale di edifici alti soggetti all'azione turbolenta del vento [MS Thesis] Italy: University of Cagliari; 2014.
[35] Cui W, Caracoglia L. Simulation and analysis of intervention costs due to wind-induced damage on tall buildings. Eng Struct 2015;87:183–97.
[36] Caracoglia L, Jones NP. Experimental derivation of the dynamic characteristics of highway light poles. In: Twenty-forth International Modal Analysis Conference (IMAC-XXIV). St. Louis, Missouri, USA; January 30-February 2, 2006, CD-ROM.
[37] Bucher C. Computational analysis of randomness in structural mechanics. London, UK: Taylor Francis Group; 2009.
[38] Der Kiureghian A. First- and second-order reliability methods. Engineering design reliability handbook. Boca Raton, Florida, USA: CRC Press; 2005.
[39] Haldar A, Mahadevan S. Reliability assessment using stochastic finite-element analysis. New York, NY, USA: John Wiley and Sons; 2000.
[40] Dragt RC, Allaix DL, Maljaars J, Tuitman JT, Salman Y, Otheguy ME. Approach to include load sequence effects in the design of an Offshore Wind Turbine substructure. In: Proceedings of the 27th International Ocean and Polar Engineering Conference, ISOPE 2017. p. 312–319.
[41] Au SK, Beck JL. Estimation of small failure probabilities in high dimensions by subset simulation. Prob Eng Mech 2001;16(4):263–77.
[42] Cheng J, Cai CS, Xiao R-C, Chen SR. Flutter reliability analysis of suspension bridges. J Wind Eng Indust Aerodyn 2005;93(10):757–75.
[43] Ge YJ, Xiang HF, Tanaka H. Application of a reliability analysis model to bridge flutter under extreme winds. J Wind Eng Indust Aerodyn 2000;86(2–3):155–67.
[44] Baldomir A, Kusano I, Jurado JA, Hernandez S. A reliability study for the Messina Bridge with respect to flutter phenomena considering uncertainties in experimental and numerical data. Comput Struct 2013;128:91–100.
[45] Piccardo G, Solari G. Generalized equivalent spectrum technique. Wind Struct 1998;1(2):161–74.
[46] Kareem A. Aerodynamic response of structures with parametric uncertainties. Struct Saf 1988;5(3):205–25.
[47] Kaimal JC, Wyngaard JC, Izumi Y, Coté OR. Spectral characteristics of surface-layer turbulence. Q J R Meteorol Soc 1972;98(417):563–89.
[48] Davenport AG. Note on the distribution of the largest value of a random function with application to gust loading. J Proc Inst Civ Eng 1964;28(2):187–96.
[49] Davenport AG. A statistical approach to the treatment of wind loading on tall masts and suspension bridges. United Kingdom: University of Bristol; 1961.
[50] Isyumov N, Alan G. Davenport's mark on wind engineering. J Wind Eng Indust Aerodyn 2012;104:12–24.
[51] EC-1.4. Eurocode 1: Actions on structures – Part 1-4: General Actions – Wind actions (prEN 1991-1-4.6). European Committee for Standardisation (CEN); 2002.
[52] Cui W, Caracoglia L. Examination of experimental variability in HFFB testing of a tall building under multi-directional winds. J Wind Eng Indust Aerodyn 2017;171:34–49.
[53] Gioffrè M, Gusella V, Materazzi AL, Venanzi I. Removable guyed mast for mobile phone networks: wind load modeling and structural response. J Wind Eng Indust Aerodyn 2004;92:463–75.
[54] Harju A, Barbiellini B, Siljamäki S, Nieminen RM, Ortiz G. Stochastic gradient approximation: an efficient method to optimize many-body wave functions. Phys Rev Lett 1997;1997(79):1173–7.
[55] Spall JC. Introduction to stochastic search and optimization: estimation, simulation

and control. Hoboken, New Jersey, USA: John Wiley and Sons; 2003.
[56] Robbins H, Monro S. Stochastic approximation method. Ann Math Stat 1951;22(3):400–7.
[57] Giaccu GF, Barbiellini B, Caracoglia L. Parametric study on the nonlinear dynamics of a three-stay cable network under stochastic free vibration. J Eng Mech, ASCE 2015;141(6):04014166.
[58] Norton T, Abdullah MM, Stephens D. Proposed methodology for performance-based vulnerability assessment of wind-excited tall buildings. In: Choi C-K, Holmes JD, Kim Y-D, Kwak HG, editors. Fourth International Conference on Advances in Wind and Structures (AWAS'08). Jeju Island, South Korea: Techno-Press, South Korea; 2008. p. 1228–46. ISBN 978-89-89693-23-9-98530.
[59] Bashor R, Kareem A. Probabilistic performance evaluation of buildings: an occupant comfort perspective. In: 12th International Conference on Wind Engineering (12-ICWE). Cairns, Australia, July 1–6, 2007. p. 1335–1342.
[60] Filliben JJ, Gurley K, Pinelli J-P, Simiu E. Fragility curves, damage matrices, and wind induced loss estimation. In: Third International Conference on 'Computer Simulation in Risk Analysis and Hazard Mitigation'. Sintra, Portugal; 2002. p. 119–126.
[61] Le V, Caracoglia L. Computationally efficient stochastic approach for the fragility analysis of vertical structures subjected to thunderstorm downburst winds. Eng Struct 2018;165:152–69.